materials

MDPI

Article

Converting Sewage Water into H_2 Fuel Gas Using Cu/CuO Nanoporous Photocatalytic Electrodes

N. M. A. Hadia [1,2,*], Ahmed Adel A. Abdelazeez [3,4], Meshal Alzaid [1], Mohamed Shaban [5,6], S. H. Mohamed [6,7], Bram Hoex [8], Ali Hajjiah [9,*] and Mohamed Rabia [5,10]

1 Physics Department, College of Science, Jouf University, Sakaka P.O. Box 2014, Saudi Arabia; mmalzaid@ju.edu.sa
2 Basic Sciences Research Unit, Jouf University, Sakaka P.O. Box 2014, Saudi Arabia
3 Nanoscale Science, University of North Carolina at Charlotte, Charlotte, NC 28223, USA; aabdelh2@uncc.edu
4 State Key Lab of Metastable Materials Science and Technology, Yanshan University, Qinhuangdao 066004, China
5 Nanophotonics and Applications Lab, Physics Department, Faculty of Science, Beni-Suef University, Beni-Suef 62514, Egypt; mssfadel@aucegypt.edu (M.S.); mohamedchem@science.bsu.edu.eg (M.R.)
6 Department of Physics, Faculty of Science, Islamic University of Madinah, Prince Naifbin Abdulaziz, Al Jamiah, Madinah 42351, Saudi Arabia; abo_95@yahoo.com
7 Physics Department, Faculty of Science, Sohag University, Sohag 82524, Egypt
8 School of Photovoltaics and Renewable Energy Engineering, University of New South Wales, Sydney, NSW 2052, Australia; b.hoex@unsw.edu.au
9 Electrical Engineering Department, College of Engineering and Petroleum, Kuwait University, Safat 13113, Kuwait
10 Nanomaterials Science Research Laboratory, Chemistry Department, Faculty of Science, Beni-Suef University, Beni-Suef 62514, Egypt
* Correspondence: nmhadia@ju.edu.sa (N.M.A.H.); ali.hajjiah@ku.edu.kw (A.H.)

Citation: Hadia, N.M.A.; Abdelazeez, A.A.A.; Alzaid, M.; Shaban, M.; Mohamed, S.H.; Hoex, B.; Hajjiah, A.; Rabia, M. Converting Sewage Water into H_2 Fuel Gas Using Cu/CuO Nanoporous Photocatalytic Electrodes. *Materials* **2022**, *15*, 1489. https://doi.org/10.3390/ma15041489

Academic Editor: Jinheung Kim

Received: 13 January 2022
Accepted: 10 February 2022
Published: 16 February 2022

Abstract: This work reports on H_2 fuel generation from sewage water using Cu/CuO nanoporous (NP) electrodes. This is a novel concept for converting contaminated water into H_2 fuel. The preparation of Cu/CuO NP was achieved using a simple thermal combustion process of Cu metallic foil at 550 °C for 1 h. The Cu/CuO surface consists of island-like structures, with an inter-distance of 100 nm. Each island has a highly porous surface with a pore diameter of about 250 nm. X-ray diffraction (XRD) confirmed the formation of monoclinic Cu/CuO NP material with a crystallite size of 89 nm. The prepared Cu/CuO photoelectrode was applied for H_2 generation from sewage water achieving an incident to photon conversion efficiency (IPCE) of 14.6%. Further, the effects of light intensity and wavelength on the photoelectrode performance were assessed. The current density (J_{ph}) value increased from 2.17 to 4.7 mA·cm^{-2} upon raising the light power density from 50 to 100 mW·cm^{-2}. Moreover, the enthalpy (ΔH*) and entropy (ΔS*) values of Cu/CuO electrode were determined as 9.519 KJ mol^{-1} and 180.4 JK^{-1}·mol^{-1}, respectively. The results obtained in the present study are very promising for solving the problem of energy in far regions by converting sewage water to H_2 fuel.

Keywords: hydrogen generation; sewage water; photocatalyst; water spiting; CuO; nonporous

1. Introduction

Photocatalytic materials represent an important class of components for potential applications in renewable-energy-related fields such as solar cells, optoelectronic, and photocatalytic H_2 production [1–4]. On the one hand, the production of H_2 gas from sewage water is a very promising field of renewable energy. This process provides H_2 gas fuel for different uses of normal life such as cooking and warming, especially in remote regions inside deserts or rural areas. Moreover, this H_2 gas is used as a fuel for airplanes and aircrafts, in addition to its normal utilization in industrial factories and companies. On the other hand, this photocatalytic reaction removes contamination (sewage water) through

conversion into fuel. In addition, the H_2 fuel is clean energy; its combustion has no side effects. The dependence of the world on this clean energy reduces the use of fossil fuels with their harmful produced gases such as CO_2, NO_x, and SO_x [5–7].

The photocatalysts applied for H_2 generation reaction must be semiconducting materials such as metal oxides, sulfides, nitrides, or organic [8,9]. Metal oxides have many benefits that qualified them to be ideal photocatalytic materials for H_2 production such as low cost, stability, and easy preparation [10,11]. There are some methods for enhancing the photocatalytic activity such as increasing the surface area (nanofibers, nanowires, and nanotubes) [12–14]. Another way to enhance the photocatalytic activity is through the use of plasmonic materials [15,16], or materials with high thermal capacity such as Cu metal. These materials are effective for light capture and cause electron localization phenomena extended over the composite semiconductor materials, after which the neighbor materials use these phenomena for the H_2 production process [17]. Previous studies examined the effect of Cu as a plasmonic material in Cu/ZnO for light capture and enhancement of the photocatalytic properties of ZnO [18].

CuO and Cu_2O are promising materials for renewable energy applications, owing to their bandgap values of 0.7–1.6 eV and 2.0–2.2 eV for CuO and Cu_2O, respectively [19,20]. These low bandgap values enable these materials to absorb most of the sunlight, which is preferable to large bandgap semiconductors that can absorb 10% to 20% of sunlight [21]. Moreover, the lower bandgap and high absorption efficiency of CuO favor its application (compared with Cu_2O) in the renewable energy field [22].

In 2014, Li et al. managed to synthesize a nanoporous CuO layer onto Cu foil through the annealing of Cu $(OH)_2$ nanowires at 500 °C under an oxygen flow. A thick Cu_2O interlayer was also formed; this annealing process formed under high oxygen pressure, which is higher than CuO dissociation pressure, so the CuO layer formed at the outer surface of the structure. The $Cu/Cu_2O/CuO$ structure is used as an electrode for glucose sensing. Sagadevan et al. prepared CuO nanoparticles via the combustion technique for various annealing temperatures (100 °C and 300 °C), with ascorbic acid used as a capping agent [23]. Ragupathi et al. prepared $CuO/g\text{-}C_3N_4$ for a water-splitting reaction, but the produced current density (Jph) and the incident photon to current conversion efficiency (IPCE) were very small [24]. Quyen et al. studied the effect of Cu on TiO_2 for the photocatalytic water splitting reaction and determined that Cu nanoparticles increased the photocatalytic effect very much and increased the rate of H_2 generation, which resulted from increasing oxygen vacancies in TiO_2 and the charge transfer process [24]. Shen et al. prepared graphite carbon nitride and decorated this material with CuO for photocatalyst application, and studied the effect of CuO for increasing the efficiency of the catalytic reaction and H_2 generation, but the rate of H_2 generation was small [25].

Most of the previous studies on CuO relied on the use of an additional sacrificing agent such as Na_2SO_3, $Na_2S_2O_3$, HCl, and NaOH [26–28]. Moreover, the H_2 rate production was limited [29–32]. Various fabrication methods of CuO have been reported such as physical sputtering, atomic layer deposition, spray pyrolysis, radiofrequency sputtering, and so on. However, these techniques have drawbacks of high-cost, long fabrication time, and complex fabrication processes [33,34].

This study provides the H_2 gas fuel from the contamination (sewage water) without using any additional electrolyte. The catalytic electrode is prepared with a low-cost combustion method without using any complex techniques. The prepared electrode has a high J_{ph} in comparison with the previous literature. The produced efficiency is promising for application of this electrode in H_2 generation from sewage water in industrial applications.

In this study, Cu/CuO photocathode, prepared by an oxidation/combustion process, was evaluated for H_2 production from a sewage water-splitting reaction without using any sacrificing agent. The influence of various factors such as light intensity and wavelength, temperature, and on/off chopped current was assessed on the photocathode performance. Finally, IPCE was estimated under different monowavelength light, and the mechanism for the sewage water splitting reaction was examined.

2. Materials and Methods

2.1. Cu/CuO Nanomaterial Preparation

Prior to sample preparation, the Cu foil was cleaned using water, soap, acetone, and ethanol under ultrasonication for 10 min each. The preparation of Cu/CuO was carried out through oxidation combustion of copper foil (99.9%, thickness 0.3 mm) in Nabertherm box furnace (Nitrex Metal Inc., St-Laurent, QC, Canada) at 550 °C for 1 h. Through this combustion process, the Cu metal is oxidized to generate CuO NP material. Then 1 cm^2 of the Cu/CuO was used as electrode for hydrogen generation under wastewater splitting reaction through electrochemical measurements.

2.2. Characterization

X-ray diffraction pattern (XRD, Malvern Panalytical Ltd., Malvern, UK) analyses were carried out using a Bruker D8 advance diffractometer using Cu Kα radiation (wavelength = 0.15418 nm). Field-emission scanning electron microscopy (FE-SEM, Hitachi, S-4800, Schaumburg, IL, USA) was used to assess the morphology. The energy dispersive X-ray analysis (EDAX, Hitachi, Schaumburg, IL, USA) elemental composition and elemental mapping were examined using the EDAX unit attached to the FE-SEM. The optical properties were examined using a double beam spectrophotometer (Perkin Elmer Lamba 950, Shelton, CT, USA).

2.3. Electrochemical Measurements

The H_2 generation reaction was carried out from sewage water solution (100 mL, pH 5.5) using a three-electrode cell, in which Cu/CuO nanomaterial (1cm^2), a graphite sheet of the same dimensions, and calomel act as working, counter, and reference electrodes, respectively, as shown in Figure 1. All measurements were carried out using a workstation (CHI660E, Tennison Hill Drive, Austin, TX, USA) in a potential range from −1 to 1 V, a xenon lamp acts as a solar simulator. Some parameters were studied such as the light intensity (25 to 100 mW·cm^{-2}), light wavelength (390 to 636 nm), on/off chopped current, and temperature on the electrode performance.

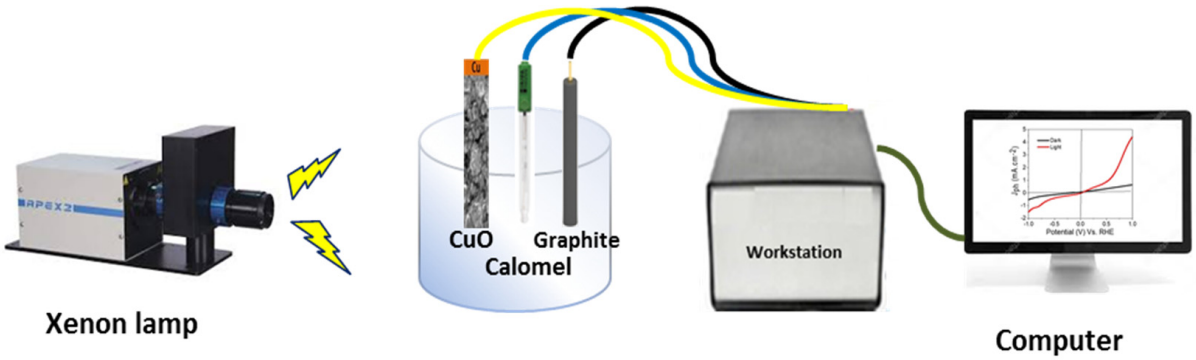

Figure 1. Schematic diagram for photoelectrochemical H_2 generation process from sewage water.

The sewage water was obtained from the drinking water and sanitation of Beni Suef city, Egypt, and the construction was confirmed using gas chromatography–mass spectrometry.

3. Results and Discussion

Morphological, Structural, and Optical Properties

The morphology of the CuO NP, prepared from Cu metal using a simple combustion process in air at 550 °C for 1 h, is displayed in Figure 2a,b. The CuO NP substrate consists of island-like structures with an inter-distance of 100 nm. Each island is highly porous with a pore diameter of about 250 nm. The formation of these pores with high homogeneous distribution on the CuO surface enlarges the surface area. This feature is beneficial for the

photocatalytic process through high light absorption efficiency, in which the porous surface acts as a cave for light absorption [7,12].

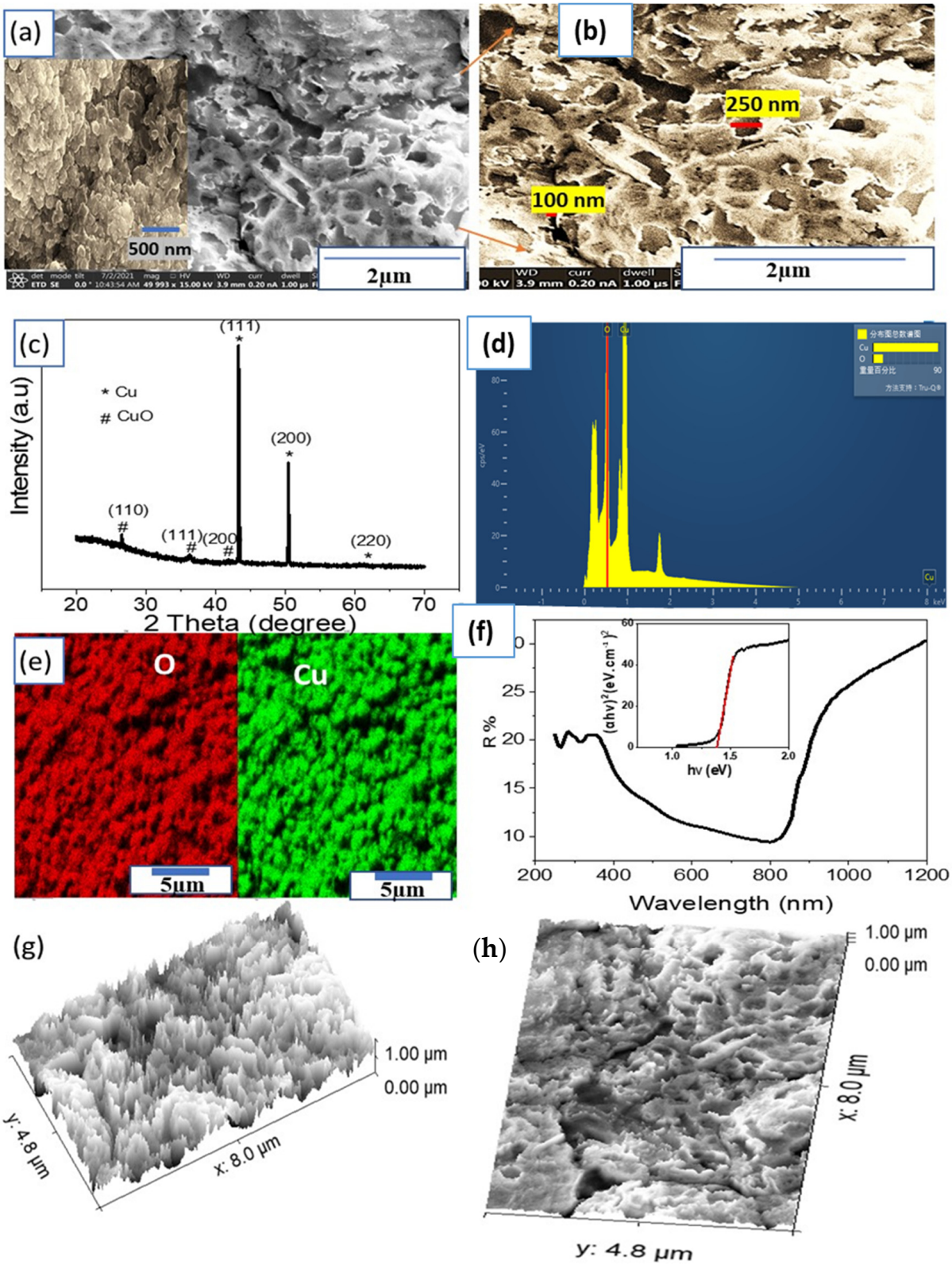

Figure 2. (**a**,**b**) FESEM images, (**c**) XRD pattern, (**d**) EDAX, (**e**) elemental mapping for O (red) and Cu (green), and (**f**) optical reflectance and bandgap (insert) of the CuO NP thin film. (**g**,**h**) The cross section and surface roughness using the modeling program (ImageJ), respectively.

Figure 2c shows the XRD pattern of the Cu/CuO sample showing the two characteristic peaks of CuO at around 35.6° and 38.5° (JCPDS #41–0254), indicating that CuO NP were formed on the copper foil [35–37]. The other three strong diffraction peaks at 43.5°, 50.7°, and 74.5° correspond to the (111), (200), and (220) reflections, respectively, of the face-centered-cubic Cu (JCPDS #02–1225) [36,38]. The crystal size of the CuO nanomaterials is calculated using the Scherrer equation [39–41], Equation (1):

$$D = 0.94\lambda / ss \cos\theta \quad (1)$$

where ß is the full width at half maximum (), λ is the X-ray wavelength (CuKα = 0.154 nm), and θ is the Bragg's angle [42]. From the equation, the average crystal size of CuO is about 89 nm.

The EDAX spectrum (Figure 2d) and EDAX mapping images (Figure 2e) confirm the formation of the CuO NP material where Cu and O peaks are obviously present. The Cu and O elements are homogeneously distributed over the whole examined area.

The optical diffuse reflectance of the CuO NP was determined using a double beam spectrophotometer, as shown in Figure 2f. It is evident that the prepared CuO NP has a high light absorption behavior in a wide optical range (Vis and near IR). This is related to the low reflectance behavior of CuO NP in these regions. The bandgap is calculated using the Kubelka–Munk equation (Equation (2)) [12], as shown in the insert of Figure 2f, where K is the molar absorption coefficient, and S is the scattering factor. From Equation (2), a bandgap of 1.38 eV was determined for the CuO thin film, which is in good agreement with a recent research study [43].

$$K/S = \frac{(1-R)^2}{2R} \quad (2)$$

The cross section and roughness is estimated using the modeling program (Image J) as shown in Figure 2g,h. From this figure, the surface roughness appears well with a surface area of 235 μm^2 in 38 μm^2.

The photoelectrochemical (PEC) activity of the Cu/CuO photoelectrode was assessed in sewage water (chemical composition in Table 1) at room temperature (25 °C) with a sweep rate of 1 mV/s under xenon lamp illumination. The PEC measurements were performed in dark and light without optical filters, as shown in Figure 3a. The broad surface area of the prepared nanotextured electrode generates a high density of electron-hole pairs when exposed to light, leading to the splitting of H_2O molecules to conduct the hydrogen electro-generation reaction. The effect of light on the Cu/CuO photoelectrode generate J_{ph} values of −0.07 and 4.7 mA·cm^{-2} at 0 and 1 V, respectively (Figure 3a), although the density of the dark current is very small for the electrode and can be ignored. Therefore, from the J_{ph} values, the Cu/CuO with the lowest photogeneration voltage (0.56 V) is a highly efficient electrode for water splitting and H_2 gas generation.

The substrate Cu metal contributes to a high density of pairs of electrons formed. This will motivate H_2O molecules to be broken to produce hydrogen when it reaches the CuO surface. The spectral overlap between CuO absorbance oscillator frequencies and the Cu metal oscillator frequency improves the produced photocurrent.

The stability (time-J_{ph} relation) of the prepared Cu/CuO photoelectrode was studied as presented in Figure 3b. At +0.1 V, the produced J_{ph} value under on and off chopped light is mentioned. From the figure, the electrode has high stability and sensitivity to light. From the magnified part in Figure 3c, the change in the J_{ph} values under on and off chopped light appears well. This confirms the high sensitivity of the electrode to light due to the high effect of the light on the electrode. The reproducibility of the electrode for four runs is shown in Figure 3d, in which the voltage–current relation shows the same behavior until four runs. This reproducibility was carried out at 30 °C and in normal light. The standard deviation (SD) value for the Cu/CuO photoelectrode is 0.3%.

Table 1. The sewerage water chemical composition used as the electrolyte for H_2 production.

Material or Element	Concentration (mg/L)
Phenols	0.015
F^-	1.0
Al^{3+}	3.0
NH_3	5.0
Hg^{2+}	0.005
Pb^{2+}	0.5
Cd^{3+}	0.05
As^{3+}	0.05
Cr^{3+}	1.0
Cu^{2+}	1.5
Ni^{3+}	0.1
Fe^{3+}	1.5
Mn^{2+}	1.0
Zn^{2+}	5.0
Ag^{+}	0.1
Ba^{3+}	2.0
Co^{2+}	2.0
Other cations	0.1
Pesticides	0.2
CN^{-1}	0.1
Industrial washing	0.5
Coli groups	4000/100 cm^3

The effect of light intensity (50 to 100 $mW{\cdot}cm^{-2}$) on the Cu/CuO photoelectrode is mentioned in Figure 4a,b. This effect appears clearly, in which the J_{ph} values increase from 2.17 to 4.7 $mA{\cdot}cm^{-2}$, directly with the light intensity until 100 $mW{\cdot}cm^{-2}$. This increase is related to the electron–hole pair formation under the increasing light intensity [44], in which many photons activate the active sites on the photocatalytic materials [45]. The J_{ph} represents the electrons collected on the surface of the photoelectrode; this J_{ph} then represented the water splitting and H_2 generation rate [46,47].

The number of photons (N) is directly proportional to the light intensity (P) as shown in Equation (3). This equation depends on other factors such as wavelength (λ), Planck constant (h), and light velocity (c). From this equation, the N per second is changed from 4×10^{21} to 8×10^{21} photon/s under light intensity from 50 to 100, $mW{\cdot}cm^{-2}$, respectively.

$$N = \lambda P/hc \quad (3)$$

The effect of the light monowavelength (390 to 636 nm) on the produced J_{ph} for Cu/CuO electrodes is presented in Figure 5a. From this figure, the J_{ph} has varied values under the monochromatic light effect. The optimum J_{ph} value is 4.6 $mA{\cdot}cm^{-2}$ at 390 nm, in which these values correspond to the optical analyses data (Figure 3). The inset figure in Figure 6a shows this relation clearly.

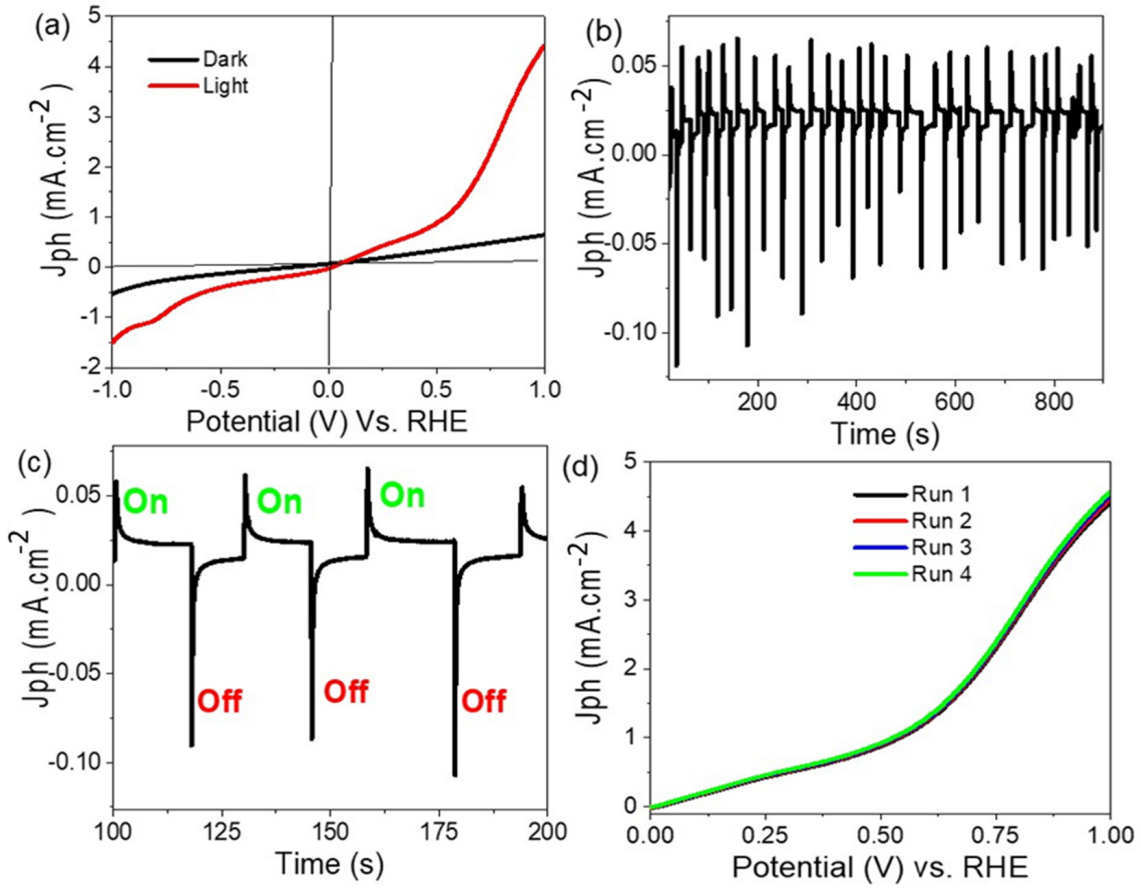

Figure 3. The voltage–current relation for (**a**) Cu/CuO and (**b**,**c**) on/off chopping current (**d**) stability.

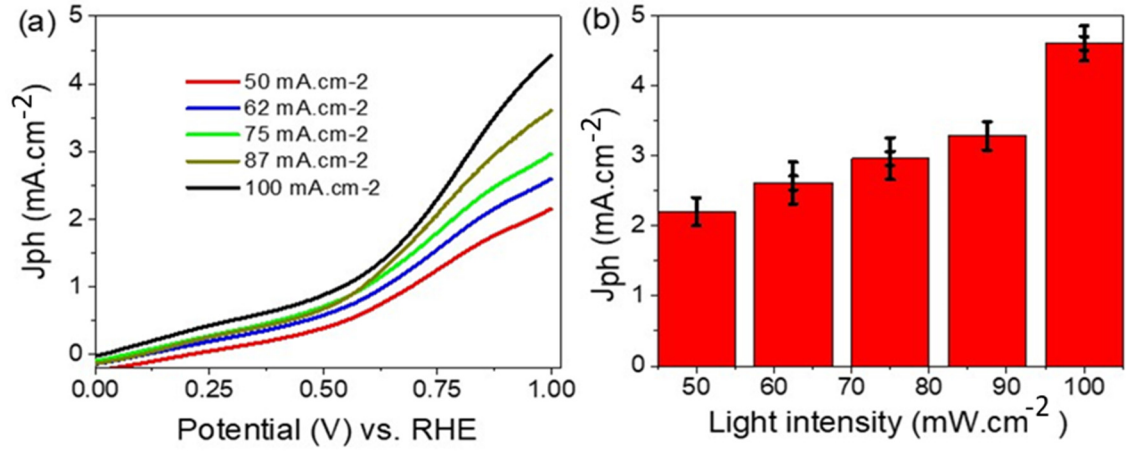

Figure 4. (**a**,**b**) The effect of light intensity on J_{ph} for the Cu/CuO photoelectrode.

The incident photon to current conversion efficiency (IPCE) represents the electrons collected on the surface of the photocatalytic materials under the photon flux (Figure 5b). This IPCE value can be calculated from the wavelength values [48], through Equation (4).

$$\mathrm{IPCE} = \frac{J_{ph}\left(\mathrm{mA{\cdot}cm^{-2}}\right){\cdot}1240\ (\mathrm{V{\cdot}nm})}{P\left(\mathrm{mW{\cdot}cm^{-2}}\right){\cdot}\lambda(\mathrm{nm})} \quad (4)$$

The IPCE is determined at 100 $\mathrm{mW{\cdot}cm^{-2}}$ for the photoelectrode Cu/CuO and presented in Figure 5b. The IPCE values very much depend on monochromatic light, in which

the optimum IPCE value is 14.6% at 390 nm. The IPCE values decrease with increasing wavelengths. Therefore, the photocatalytic electrode has the ability for sewage water splitting and H_2 generation with 14.6% efficiency. This high value was produced without using any additional electrolyte and infers that the electrode converts the sewage water into H_2 and O_2 with high efficiency in comparison with other previous literature [29,49–53].

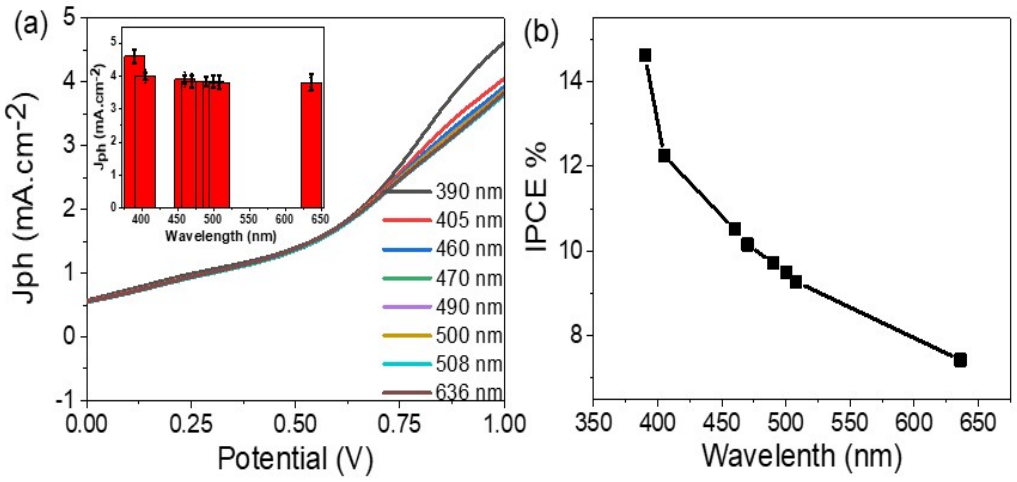

Figure 5. (**a**) The potential J_{ph} relation under different wavelengths (390 to 636 nm) illumination and (**b**) the IPCE for Cu/CuO electrode.

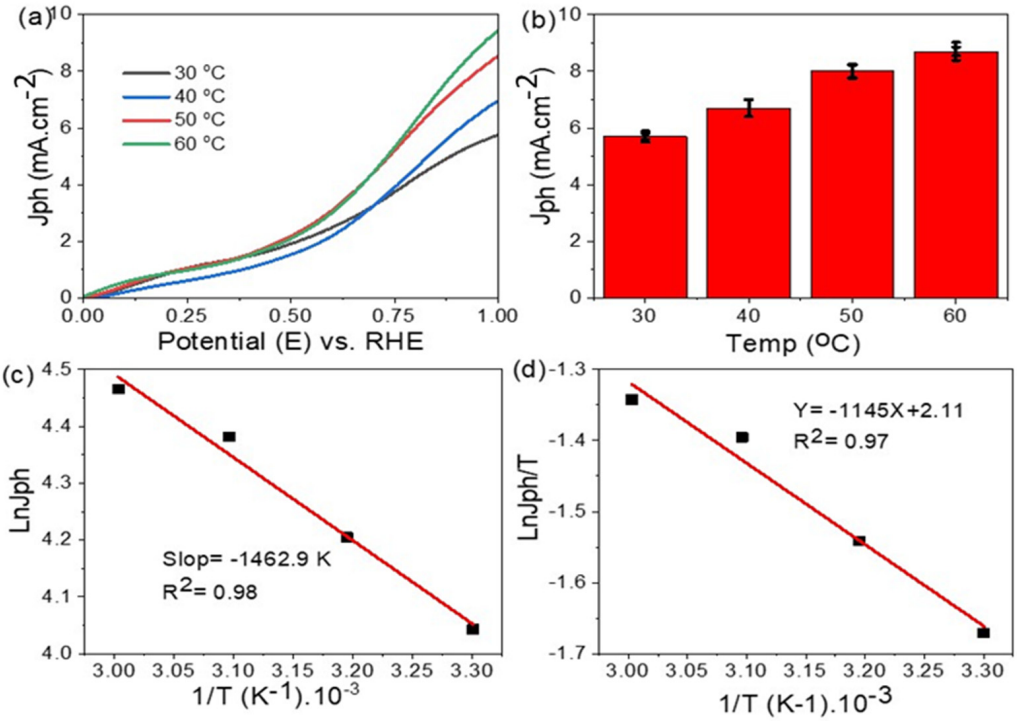

Figure 6. (**a**,**b**) The temperature effect, (**c**) activation energy, and (**d**) heat of reaction for Cu/CuO electrodes.

There is an inverse relationship between the number of photons and IPCE. The optimum values occur at low wavelengths, in which the light has a high frequency for transferring most electrons to the conducting band, so the J_{ph} value increases, and thereby the H_2 production increases [54].

The water splitting reaction for the H_2 generation process using the Cu/CuO photoelectrode under different temperatures is mentioned in Figure 6a. The J_{ph} values increase from 4.7 to 8.8 mA·cm^{-2} with increasing the temperature from 30 to 60 °C, respectively.

This increasing behavior of the J_{ph} indicates the high mobility of the sewage water ions with increasing temperature, in which the high ionic mobility facilitates the H_2 and O_2 generation in both sides of the electrochemical cell. So increasing the J_{ph} values with the temperature indicates an increase in the H_2 generation rate [55,56].

The activation energy (E_a) for the H_2 generation can be calculated under different temperatures using the Arrhenius equation (Equation (5)) [57]. This E_a depends on the rate of collisions (k is the rate constant) and temperature values in Kelvin (T) using the universal gas constant (R) and Arrhenius constant (A) as the standard constant. From the E_a value, the initiator temperature for starting the splitting reaction is determined [58–60]. E_a values are obtained from slope of ln J_{ph} versus 1/T as shown in Figure 6c. The E_a value is 11.8 KJ mol^{-1} for the electrode. The small value of the water splitting reaction indicates the splitting occurs easily for the H_2 and O_2 evolution [61].

For calculating the enthalpy (ΔH*) and entropy (ΔS*), Equation (6) is applied (Eyring equation) [62,63]. This equation is similar to the Arrhenius equation, but it contains additional parameters and uses additional constants, in which k_B is the Boltzman constant and h is the Planck constant. By applying this equation for the sewage splitting reaction of the Cu/CuO photoelectrode, ΔH* and ΔS* values are obtained as 9.519 kJ mol^{-1} and 180.4 $JK^{-1}{\cdot}mol^{-1}$, respectively (Figure 6c).

Moreover, the H_2 moles are calculated from the Faraday equation, Equation (7) [64,65], under time change (dt), using the Faraday constant (F). The estimated H_2 mole for the Cu/CuO photoelectrode is 60 μmol h^{-1} cm^{-2}. In addition, a comparison between the present study and the previously reported literature is added in Table 2.

$$k = Ae^{-Ea/RT} \tag{5}$$

$$k = T{\cdot}\frac{kB}{h}{\cdot}e^{\Delta S/R}{\cdot}e^{-\Delta H/RT} \tag{6}$$

$$H_2\ \text{mole} = \int_0^t J_{ph}{\cdot}dt/F \tag{7}$$

The mechanism of the CuO photocatalytic materials for the sewage water-splitting reaction is based on the effect of incident light on the motivation of the photoelectrons from the CuO NP material that resulted from the energy band changes (Figure 7). The photoelectrons generated under the effect of light incidence have two steps. First, electron-hole generation, in which the generated electrons leave the holes and transfer to the upper level. The second step is the localized surface plasmonic resonance (LSPR); this resonance process causes the energy transfer [66]. These two steps occurred easily due to the small CuO band gap of 1.39 eV in addition to the absence of depletion regions inside the Cu and CuO nanomaterials. Therefore, the results are the transfer of electrons from the Cu to CuO without any restrictions, and the continuous electrons flow is carried out without any restrictions [67]. These hot electrons cause the generation of J_{ph} under the applied potential [68–70]. The experimental image of electrons transfer processes is represented in the optical analyses (Figure 3) and the electrochemical measurements under various effects such as light intensity and light wavelengths. The Cu metal substrate has plasmonic properties that cause the light capture and electron resonance process [52] that motivates the CuO nanomaterials and generates electrons over their surface [71–73]. These electrons are represented in J_{ph} values and the H_2 generation reaction rate [74,75].

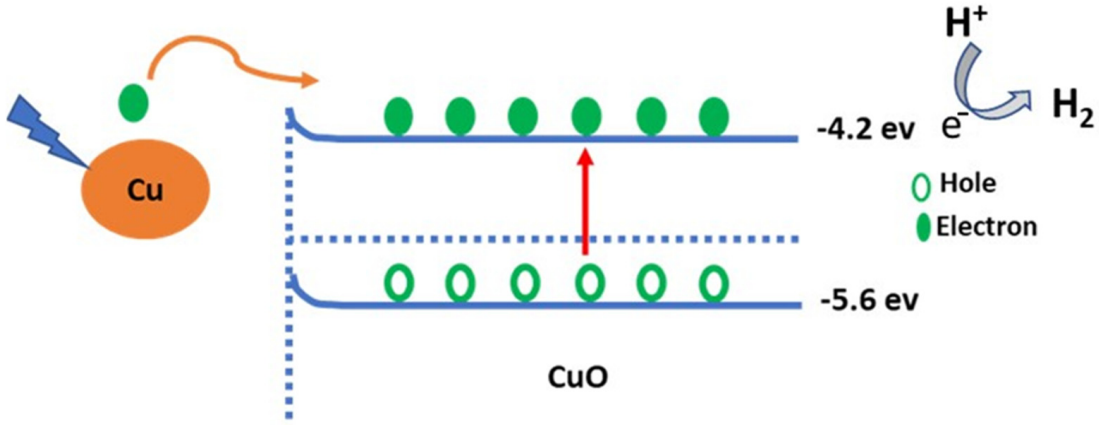

Figure 7. Schematic diagram of the sewage water splitting mechanism.

Table 2. Comparison between the present study and the previous reported literature; electrolyte used, J_{ph}, and IPCE values.

Photoelectrode	Electrolyte	J_{ph} (mA/cm^2)	Applied Voltage (V)	IPCE% (390 nm)	Light Source
g-C_3N4-CuO [23]	NaOH	0.01	1.6	-	300 W xenon lamp
CuO-C/TiO_2 [76]	glycerol	0.001	−0.5	-	300 W xenon lamp
CuO nanowire [77]	Na_2SO_4	1.5	−0.5	-	simulated AM1.5 illumination
CuO nanostructure [78]	KOH	1	−1.2	-	White light
CuO thin films [79]	Na_2SO_4	2.5	0	3.1	Solar simulator 1.5 global (AM 1.5G)
CuO nanocrystals [80]	Na_2SO_4	1.1	−0.5	8.7	Xenon lamp light
TiO_2/CdS/PbS [81]	$Na_2S/Na_2S_2O_3$	2	0.2	4	AM 1.5G illumination
GaN [82]	HBr	0.6	+1	8	Sunlight
ZnO/TiO_2/FeOOH [83]	$Na_2S_2O_3$	1.59	0.8	-	A 150 W xenon lamp
SnO_2/TiO_2 [84]	$Na_2S_2O_3$	0.4	0.6	-	1 Sun (100 mW cm^{-2})
Au/PbS/Ro-GO/PANI [85]	$Na_2S_2O_3$	1.1	+1	10	400 W xenon lamp
TiN-TiO_2 [86]	NaOH	3.0×10^{-4}	0.2	0.03	Solar simulator (150 mW cm^{-2})
$BiFeO_3$ [29]	NaOH	0.1	1.6	0.21	1 sun (AM 1.5G solar spectrum)
ITO/VO2 [50]	$Na_2S_2O_3$	1.5	+1	4	400 W metal halid
PrFeO [49]	Na_2SO_4	0.130	−0.6	-	Simulated sunlight
Poly(3-aminobenzoic acid) frame [53]	H_2SO_4	1.2	1.6	-	150 W xenon lamp
Cu/CuO (Present work)	Sewage water	4.7	+1	14.6	Simulated sunlight

4. Conclusions

This work provides promising results in support of H_2 production from sewage water using a CuO NP photoelectrode. All the analyses were carried out for confirming the chemical structure, morphology, and optical properties of the prepared CuO NP. From the SEM, the prepared materials have nanoporous features that look like small islands with diameters of about 300–400 nm, with each island composed of a package of small nanoporous particles. XRD confirmed the monoclinic CuO crystalline phase with crystallite size of 89 nm. The obtained optical band gap value for CuO NP was 1.39 eV. The sewage water was used as a source of H_2 gas produced by the Cu/CuO photoelectrode. The J_{ph} value was changed from 2.17 to 4.7 mA·cm^{-2} upon increasing the light power density from

50 to 100 mW·cm^{-2}, respectively. The IPCE was changed under the effect of monochromatic light, in which the optimum IPCE value was 14.6% at 390 nm. Moreover, the effect of on and off chopped current was studied that confirms the motivation of the photocatalyst under light incidence. The sewage water splitting thermodynamics were studied, in which the enthalpy (ΔH*) and entropy (ΔS*) values for the Cu/CuO electrode were 9.519 kJ·mol^{-1} and 180.4 JK^{-1}·mol^{-1}, respectively. A mechanism was proposed to explain the relationship between the incidence light and the J_{ph} values of the H_2 generation rate.

Author Contributions: Conceptualization, A.A.A.A., N.M.A.H., M.A., A.H. and M.R.; methodology, software, validation, formal analysis, investigation, resources, data curation, writing—original draft preparation, visualization, supervision, and project administration, S.H.M., B.H., A.A.A.A., M.R., M.S., A.H. and N.M.A.H.; synthetized photoelectrode, S.H.M., B.H., A.A.A.A., M.R. and B.H.; writing—review and editing, A.A.A.A., M.R., N.M.A.H., M.A., M.R., A.H. and M.S.; funding, N.M.A.H., A.H. and M.A. All authors have read and agreed to the published version of the manuscript.

Funding: The authors extend their appreciation to the Deanship of Scientific Research at Jouf University for funding this work through a research grant (no. DSR-2021-03-0318). Also, we would like to thank Kuwait University for their technical and financial support on this work.

Institutional Review Board Statement: Not applicable.

Informed Consent Statement: Not applicable.

Data Availability Statement: The data that support the findings of this study are available from the corresponding author upon reasonable request.

Conflicts of Interest: The authors declare that they have no conflict of interest.

References

1. Nishiyama, H.; Yamada, T.; Nakabayashi, M.; Maehara, Y.; Yamaguchi, M.; Kuromiya, Y.; Nagatsuma, Y.; Tokudome, H.; Akiyama, S.; Watanabe, T.; et al. Photocatalytic solar hydrogen production from water on a 100-m^2 scale. *Nature* **2021**, *598*, 304–307. [CrossRef]
2. Domen, K.; Hisatomi, T. Reaction systems for solar hydrogen production via water splitting with particulate semiconductor. *Nat. Catal.* **2019**, *2*, 387–399. [CrossRef]
3. Pagliaro, M. Preparing for the future: Solar energy and bioeconomy in the United Arab Emirates. *Energy Sci. Eng.* **2019**, *7*, 1451–1457. [CrossRef]
4. Takata, T. Photocatalytic water splitting with quantum efficiency of almost unity. *Nature* **2020**, *581*, 411–414. [CrossRef]
5. Mohamed, F.; Rabia, M.; Shaban, M. Synthesis and characterization of biogenic iron oxides of different nanomorphologies from pomegranate peels for efficient solar hydrogen production. *J. Mater. Res. Technol.* **2020**, *9*, 4255–4271. [CrossRef]
6. Shaban, M.; Ali, S.; Rabia, M. Design and application of nanoporous graphene oxide film for CO_2, H_2, and C_2H_2 gases sensing. *J. Mater. Res. Technol.* **2019**, *8*, 4510–4520. [CrossRef]
7. Elsayed, A.M.; Rabia, M.; Shaban, M.; Aly, A.H.; Ahmed, A.M. Preparation of hexagonal nanoporous $Al_2O_3/TiO_2/TiN$ as a novel photodetector with high efficiency. *Sci. Rep.* **2021**, *11*, 17572.
8. Kang, Z.; Cheng, Y.; Zheng, Z.; Cheng, F.; Chen, Z.; Li, L.; Tan, X.; Xiong, L.; Zhai, T.; Gao, Y. MoS_2-Based photodetectors powered by asymmetric contact structure with large work function difference. *Nano-Micro Lett.* **2019**, *11*, 1–12. [CrossRef]
9. Lee, J.H.; Lee, W.W.; Yang, D.W.; Chang, W.J.; Kwon, S.S.; Park, W. Il anomalous photovoltaic response of graphene-on-GaN schottky photodiodes. *ACS Appl. Mater. Interfaces* **2018**, *10*, 14170–14174. [CrossRef] [PubMed]
10. Abdelazeez, A.A.A.; El-Fatah, G.A.; Shaban, M.; Ahmed, A.M.; Rabia, M. ITO/Poly-3-Methylaniline/Au Electrode for Electrochemical Water Splitting and Dye Removal. *ECS J. Solid State Sci. Technol.* **2021**, *10*, 123009. [CrossRef]
11. Rabia, M.; Mohamed, H.S.H.; Shaban, M.; Taha, S. Preparation of polyaniline/PbS core-shell nano/microcomposite and its application for photocatalytic H_2 electrogeneration from H_2O. *Sci. Rep.* **2018**, *8*, 1107. [CrossRef]
12. Mohamed, H.S.H.; Rabia, M.; Zhou, X.G.; Qin, X.S.; Khabiri, G.; Shaban, M.; Younus, H.A.; Taha, S.; Hu, Z.Y.; Liu, J.; et al. Phase-junction Ag/TiO_2 nanocomposite as photocathode for H_2 generation. *J. Mater. Sci. Technol.* **2021**, *83*, 179–187. [CrossRef]
13. Nikolaidis, P.; Poullikkas, A. A comparative overview of hydrogen production processes. *Renew. Sustain. Energy Rev.* **2017**, *67*, 597–611. [CrossRef]
14. Almohammedi, A.; Shaban, M.; Mostafa, H.; Rabia, M. Nanoporous TiN/TiO_2/Alumina Membrane for Photoelectrochemical Hydrogen Production from Sewage Water. *Nanomaterials* **2021**, *11*, 2617. [CrossRef]
15. Zhang, X.; Li, J.; Yang, W.; Leng, B.; Niu, P.; Jiang, X.; Liu, B. High-performance flexible ultraviolet photodetectors based on AZO/ZnO/PVK/PEDOT:PSS heterostructures integrated on human hair. *ACS Appl. Mater. Interfaces* **2019**, *11*, 24459–24467. [CrossRef] [PubMed]

16. Kim, J.; Lee, H.C.; Kim, K.H.; Hwang, M.S.; Park, J.S.; Lee, J.M.; So, J.P.; Choi, J.H.; Kwon, S.H.; Barrelet, C.J.; et al. Photon-triggered nanowire transistors. *Nat. Nanotechnol.* **2017**, *12*, 963–968. [CrossRef]
17. Zhang, X.; Liu, Q.; Liu, B.; Yang, W.; Li, J.; Niu, P.; Jiang, X. Giant UV photoresponse of a GaN nanowire photodetector through effective Pt nanoparticle coupling. *J. Mater. Chem. C* **2017**, *5*, 4319–4326. [CrossRef]
18. Li, M.; Yu, M.; Su, D.; Zhang, J.; Jiang, S.; Wu, J.; Wang, Q.; Liu, S. Ultrahigh responsivity UV photodetector based on Cu nanostructure/ZnO QD hybrid architectures. *Small* **2019**, *15*, 1901606. [CrossRef] [PubMed]
19. Schultze, J.W.; Lohrengel, M.M. Stability, reactivity and breakdown of passive films. Problems of recent and future research. *Electrochim. Acta* **2000**, *45*, 2499–2513. [CrossRef]
20. Basnet, P.; Zhao, Y. Tuning the CuxO nanorod composition for efficient visible light induced photocatalysis. *Catal. Sci. Technol.* **2016**, *6*, 2228–2238. [CrossRef]
21. Chiang, C.Y.; Shin, Y.; Aroh, K.; Ehrman, S. Copper oxide photocathodes prepared by a solution based process. *Int. J. Hydrogen Energy* **2012**, *37*, 8232–8239. [CrossRef]
22. Chiang, C.-Y.; Chang, M.-H.; Liu, H.-S.; Tai, C.Y.; Ehrman, S. Process Intensification in the production of photocatalysts for solar hydrogen generation. *Ind. Eng. Chem. Res.* **2012**, *51*, 5207–5215. [CrossRef]
23. Ragupathi, V.; Raja, M.A.; Panigrahi, P.; Ganapathi Subramaniam, N. CuO/g-C_3N_4 nanocomposite as promising photocatalyst for photoelectrochemical water splitting. *Optik* **2020**, *208*, 164569. [CrossRef]
24. Thi Quyen, V.; Jitae, K.; Thi Huong, P.; Thi Thu Ha, L.; My Thanh, D.; Minh Viet, N.; Quang Thang, P. Copper doped titanium dioxide as a low-cost visible light photocatalyst for water splitting. *Sol. Energy* **2021**, *218*, 150–156. [CrossRef]
25. Chen, J.; Shen, S.; Guo, P.; Wang, M.; Wu, P.; Wang, X.; Guo, L. In-situ reduction synthesis of nano-sized Cu_2O particles modifying g-C_3N_4 for enhanced photocatalytic hydrogen production. *Appl. Catal. B Environ.* **2014**, *152–153*, 335–341. [CrossRef]
26. Teixeira, G.F.; Silva Junior, E.; Vilela, R.; Zaghete, M.A.; Colmati, F. Perovskite Structure Associated with Precious Metals: Influence on Heterogenous Catalytic Process. *Catalysts* **2019**, *9*, 721. [CrossRef]
27. Mishra, M.; Chun, D.M. α-Fe_2O_3 as a photocatalytic material: A review. *Appl. Catal. A Gen.* **2015**, *498*, 126–141.
28. Acar, C.; Dincer, I.; Naterer, G.F. Review of photocatalytic water-splitting methods for sustainable hydrogen production. *Int. J. Energy Res.* **2016**, *40*, 1449–1473.
29. Liu, G.; Karuturi, S.K.; Chen, H.; Wang, D.; Ager, J.W.; Simonov, A.N.; Tricoli, A. Enhancement of the photoelectrochemical water splitting by perovskite $BiFeO_3$ via interfacial engineering. *Sol. Energy* **2020**, *202*, 198–203. [CrossRef]
30. Wang, Z.; Cao, D.; Wen, L.; Xu, R.; Obergfell, M.; Mi, Y.; Zhan, Z.; Nasori, N.; Demsar, J.; Lei, Y. Manipulation of charge transfer and transport in plasmonic-ferroelectric hybrids for photoelectrochemical applications. *Nat. Commun.* **2016**, *7*, 1–8. [CrossRef]
31. Davies, J.; du Preez, S.P.; Bessarabov, D.G. On-Demand Hydrogen Generation by the Hydrolysis of Ball-Milled Aluminum– Bismuth – Zinc Composites. *Materials* **2022**, *15*, 1197. [CrossRef] [PubMed]
32. Chen, M.; Chou, S.-F.; Blaabjerg, F.; Davari, P. Overview of Power Electronic Converter Topologies Enabling Large-Scale Hydrogen Production via Water Electrolysis. *Appl. Sci.* **2022**, *12*, 1906. [CrossRef]
33. Chiang, C.Y.; Aroh, K.; Franson, N.; Satsangi, V.R.; Dass, S.; Ehrman, S. Copper oxide nanoparticle made by flame spray pyrolysis for photoelectrochemical water splitting—Part II. Photoelectrochemical study. *Int. J. Hydrogen Energy* **2011**, *36*, 15519–15526. [CrossRef]
34. Guo, X.; Diao, P.; Xu, D.; Huang, S.; Yang, Y.; Jin, T.; Wu, Q.; Xiang, M.; Zhang, M. CuO/Pd composite photocathodes for photoelectrochemical hydrogen evolution reaction. *Int. J. Hydrogen Energy* **2014**, *39*, 7686–7696. [CrossRef]
35. Zúñiga, A.; Fonseca, L.; Souza, J.A.; Rivaldo-Gomez, C.; Pomar, C.D.; Criado, D. Anomalous ferromagnetic behavior and size effects in CuO nanowires. *J. Magn. Magn. Mater.* **2019**, *471*, 77–81. [CrossRef]
36. Zhan, W.; Chen, Z.; Hu, J.; Chen, X. Vertical CuO nanowires array electrodes: Visible light sensitive photoelectrochemical biosensor of ethanol detection. *Mater. Sci. Semicond. Process.* **2018**, *85*, 90–97. [CrossRef]
37. Mahmoodi, A.; Solaymani, S.; Amini, M.; Nezafat, N.B.; Ghoranneviss, M. Structural, morphological and antibacterial characterization of CuO nanowires. *Silicon* **2017**, *10*, 1427–1431. [CrossRef]
38. Kim, J.-H.; Katoch, A.; Choi, S.-W.; Kim, S.S. Growth and sensing properties of networked p-CuO nanowires. *Sensors Actuators B. Chem.* **2015**, *212*, 190–195. [CrossRef]
39. Shaban, M.; Rabia, M.; Fathallah, W.; El-Mawgoud, N.A.; Mahmoud, A.; Hussien, H.; Said, O. Preparation and characterization of polyaniline and Ag/polyaniline composite nanoporous particles and their antimicrobial activities. *J. Polym. Environ.* **2017**, *26*, 434–442. [CrossRef]
40. Abukhadra, M.R.; Rabia, M.; Shaban, M.; Verpoort, F. Heulandite/polyaniline hybrid composite for efficient removal of acidic dye from water; kinetic, equilibrium studies and statistical optimization. *Adv. Powder Technol.* **2018**, *29*, 2501–2511. [CrossRef]
41. Fadel, M.S.S.; Rabia, M.; Ezzat, S.; Mansour, N.; Saeed, E.; Sayyah, S.M. Effect of annealing temperature on VO_2(M)/ITO film nanomaterials for thermochromic smart windows application and study its contact angle. *J. Nanophotonics* **2018**, *12*, 016009. [CrossRef]
42. Ahmed, M.A.; Rabia, M.; Shaban, M. The structure and photoelectrochemical activity of Cr-doped PbS thin films grown by chemical bath deposition. *RSC Adv.* **2020**, *10*, 14458–14470. [CrossRef]
43. Ravichandran, A.T.; Dhanabalan, K.; Vasuhi, A.; Chandramohan, R.; Mantha, S. Morphology, bandgap, and grain size tailoring in Cu_2O thin film by SILAR method. *IEEE Trans. Nanotechnol.* **2015**, *14*, 108–112. [CrossRef]

44. Yang, L.; Liu, Z. Study on light intensity in the process of photocatalytic degradation of indoor gaseous formaldehyde for saving energy. *Energy Convers. Manag.* **2007**, *48*, 882–889. [CrossRef]
45. Baniasadi, E.; Dincer, I.; Naterer, G.F. Measured effects of light intensity and catalyst concentration on photocatalytic hydrogen and oxygen production with zinc sulfide suspensions. *Int. J. Hydrogen Energy* **2013**, *38*, 9158–9168. [CrossRef]
46. Sayyah, S.M.; Shaban, M.; Rabia, M. A sensor of m-toluidine/m-cresol polymer film for detection of lead ions by potentiometric methods. *Sens. Lett.* **2016**, *14*, 522–529. [CrossRef]
47. Sayyah, S.M.; Shaban, M.; Khaliel, A.B.; Rabia, M. Electropolymerization of M-Cresol on Platinum Electrode from Aqueous Acidic Solution. *Int. J. Chem.* **2014**, *35*, 2051–2732.
48. Razek, S.A.; Popeil, M.R.; Wangoh, L.; Rana, J.; Suwandaratne, N.; Andrews, J.L.; Watson, D.F.; Banerjee, S.; Piper, L.F.J. Designing catalysts for water splitting based on electronic structure considerations. *Electron. Struct.* **2020**, *2*, 023001. [CrossRef]
49. Freeman, E.; Kumar, S.; Thomas, S.R.; Pickering, H.; Fermin, D.J.; Eslava, S. $PrFeO_3$ Photocathodes prepared through spray pyrolysis. *ChemElectroChem* **2020**, *7*, 1365–1372. [CrossRef]
50. Rabia, M.; Shaban, M.; Jibali, B.M.; Abdelkhaliek, A.A. Effect of Annealing Temperature on the Photoactivity of ITO/VO_2 (M)/Au Film Electrodes for Water Splitting. *J. Nanosci. Nanotechnol.* **2020**, *20*, 4120–4130. [CrossRef] [PubMed]
51. Potashnikov, V.; Golub, A.; Brody, M.; Lugovoy, O. Decarbonizing Russia: Leapfrogging from Fossil Fuel to Hydrogen. *Energies* **2022**, *15*, 683. [CrossRef]
52. Xiao, X.; Engelbrekt, C.; Zhang, M.; Li, Z.; Ulstrup, J.; Zhang, J.; Si, P. A straight forward approach to electrodeposit tungsten disulfide/poly(3,4-ethylenedioxythiophene) composites onto nanoporous gold for the hydrogen evolution reaction. *Appl. Surf. Sci.* **2017**, *410*, 308–314. [CrossRef]
53. Modibane, K.D.; Waleng, N.J.; Ramohlola, K.E.; Maponya, T.C.; Monama, G.R.; Makgopa, K.; Hato, M.J. Poly(3-aminobenzoic acid) Decorated with Cobalt Zeolitic Benzimidazolate Framework for Electrochemical Production of Clean Hydrogen. *Polymers* **2020**, *12*, 1581. [CrossRef] [PubMed]
54. Shaban, M.; Ahmed, A.M.; Abdel-Rahman, E.; Hamdy, H. Tunability and sensing properties of plasmonic/1d photonic crystal. *Sci. Rep.* **2017**, *7*, 1–10. [CrossRef]
55. Sayyah, S.M.; Shaban, M.; Rabia, M. Electropolymerization of *m*-toluidin on platinum electrode from aqueous acidic solution and character of the obtained polymer. *Adv. Polym. Technol.* **2018**, *37*, 126–136. [CrossRef]
56. Sayyah, E.S.M.; Shaban, M.; Rabia, M. A sensor of m-cresol nanopolymer/Pt-electrode film for detection of lead ions by potentiometric methods. *Adv. Polym. Technol.* **2018**, *37*, 1296–1304. [CrossRef]
57. Arrhenius, S. Über die Dissociationswärme und den Einfluss der Temperatur auf den Dissociationsgrad der Elektrolyte. *Z. Phys. Chem.* **1889**, *7*, 1. [CrossRef]
58. Awad, M.A.; Shaban, M.; Rabia, M. The efficiency of M (M = Li, Na, or Cs) doped CdS nanomaterials in optoelectronic applications. *Int. J. Energy Res.* **2022**. [CrossRef]
59. Rabia, M.; Mohamed, S.H.; Zhao, H.; Shaban, M.; Lei, Y.; Ahmed, A.M. TiO_2/TiOxNY hollow mushrooms-like nanocomposite photoanode for hydrogen electrogeneration. *J. Porous Mater.* **2020**, *27*, 133–139. [CrossRef]
60. Shaban, M.; Rabia, M.; Eldakrory, M.G.; Maree, R.M.; Ahmed, A.M. Efficient photoselectrochemical hydrogen production utilizing of $APbI_3$ (A = Na, Cs, and Li) perovskites nanorods. *Int. J. Energy Res.* **2021**, *45*, 7436–7446. [CrossRef]
61. Rabia, M.; Shaban, M.; Adel, A.; Abdel-Khaliek, A.A. Effect of plasmonic au nanoparticles on the photoactivity of polyaniline/indium tin oxide electrodes for water splitting. *Environ. Prog. Sustain. Energy* **2019**, *38*, 13171. [CrossRef]
62. Eyring, H. The activated complex in chemical reactions. *J. Chem. Phys.* **1935**, *3*, 63–71. [CrossRef]
63. Shaban, M.; Benghanem, M.; Almohammedi, A.; Rabia, M. Optimization of the Active Layer P3HT:PCBM for Organic Solar Cell. *Coatings* **2021**, *11*, 863. [CrossRef]
64. Helmy, A.; Rabia, M.; Shaban, M.; Ashraf, A.M.; Ahmed, S.; Ahmed, A.M. Graphite/rolled graphene oxide/carbon nanotube photoelectrode for water splitting of exhaust car solution. *Int. J. Energy Res.* **2020**, *44*, 7687–7697. [CrossRef]
65. Mohamed, H.S.H.; Rabia, M.; Shaban, M.; Taha, S. Controlled synthesis of CdS nanoflowers thin films for H_2 electro-generation. *Mater. Sci. Semicond. Process.* **2020**, *120*, 105307. [CrossRef]
66. Koya, A.N.; Zhu, X.; Ohannesian, N.; Yanik, A.A.; Alabastri, A.; Proietti Zaccaria, R.; Krahne, R.; Shih, W.C.; Garoli, D. Nanoporous metals: From plasmonic properties to applications in enhanced spectroscopy and photocatalysis. *ACS Nano* **2021**, *15*, 6038–6060. [CrossRef] [PubMed]
67. Podder, S.; Pal, A.R. Plasmonic visible-NIR photodetector based on hot electrons extracted from nanostructured titanium nitride. *J. Appl. Phys.* **2019**, *126*, 083108. [CrossRef]
68. Hussain, A.A.; Sharma, B.; Barman, T.; Pal, A.R. Self-powered broadband photodetector using plasmonic titanium nitride. *ACS Appl. Mater. Interfaces* **2016**, *8*, 4258–4265. [CrossRef] [PubMed]
69. Hussain, A.A.; Pal, A.R.; Patil, D.S. An efficient fast response and high-gain solar-blind flexible ultraviolet photodetector employing hybrid geometry. *Appl. Phys. Lett.* **2014**, *104*, 193301. [CrossRef]
70. Jiang, L.; Zhou, G.; Mi, J.; Wu, Z. Fabrication of visible-light-driven one-dimensional anatase TiO_2/Ag heterojunction plasmonic photocatalyst. *Catal. Commun.* **2012**, *24*, 48–51. [CrossRef]
71. Cao, Q.; Yu, J.; Cao, Y.; Delaunay, J.J.; Che, R. Unusual effects of vacuum annealing on large-area Ag_3PO_4 microcrystalline film photoanode boosting cocatalyst- and scavenger-free water splitting. *J. Mater.* **2021**, *7*, 929–939. [CrossRef]

72. Zhu, L.Y.; Yuan, K.; Yang, J.G.; Ma, H.P.; Wang, T.; Ji, X.M.; Feng, J.J.; Devi, A.; Lu, H.L. Fabrication of heterostructured p-CuO/n-SnO_2 core-shell nanowires for enhanced sensitive and selective formaldehyde detection. *Sens. Actuators B Chem.* **2019**, *290*, 233–241. [CrossRef]
73. Cao, Q.; Hao, S.; Wu, Y.; Pei, K.; You, W.; Che, R. Interfacial charge redistribution in interconnected network of Ni_2P–Co_2P boosting electrocatalytic hydrogen evolution in both acidic and alkaline conditions. *Chem. Eng. J.* **2021**, *424*, 130444. [CrossRef]
74. Sayyah, S.M.; Shaban, M.; Rabia, M. M-toluidine polymer film coated platinum electrode as a pH sensor by potentiometric methods. *Sens. Lett.* **2015**, *13*, 961–966. [CrossRef]
75. Sayyah, S.M.; Shaban, M.; Rabia, M. A High-sensitivity potentiometric mercuric ion sensor based on m-toluidine films. *IEEE Sens. J.* **2016**, *16*, 1541–1548. [CrossRef]
76. Huang, X.; Zhang, M.; Sun, R.; Long, G.; Liu, Y.; Zhao, W. Enhanced hydrogen evolution from CuOx-C/TiO_2 with multiple electron transport pathways. *PLoS ONE* **2019**, *14*, 0215339. [CrossRef]
77. Li, J.; Jin, X.; Li, R.; Zhao, Y.; Wang, X.; Liu, X.; Jiao, H. Copper oxide nanowires for efficient photoelectrochemical water splitting. *Appl. Catal. B Environ.* **2019**, *240*, 1–8. [CrossRef]
78. Baran Aydin, E. Fabrication and characterization of CuO nanostructures: Applications in electrocatalytic hydrogen production. *Çukurova Univ. J. Fac. Eng. Archit.* **2020**, *35*, 127–138.
79. Masudy-Panah, S.; Moakhar, R.S.; Chua, C.S.; Tan, H.R.; Wong, T.I.; Chi, D.; Dalapati, G.K. Nanocrystal Engineering of sputter-grown CuO photocathode for visible-light-driven electrochemical water splitting. *ACS Appl. Mater. Interfaces* **2016**, *8*, 1206–1213. [CrossRef] [PubMed]
80. Uchiyama, H.; Isobe, K.; Kozuka, H. Preparation of porous CuO films from $Cu(NO_3)_2$ aqueous solutions containing poly(vinylpyrrolidone) and their photocathodic properties. *RSC Adv.* **2017**, *7*, 18014–18018. [CrossRef]
81. Jin, L.; Al Otaibi, B.; Benetti, D.; Li, S.; Zhao, H.; Mi, Z.; Vomiero, A.; Rosei, F. Near-infrared colloidal quantum dots for efficient and durable photoelectrochemical solar-driven hydrogen production. *Adv. Sci.* **2016**, *3*, 1500345. [CrossRef]
82. Ebaid, M.; Kang, J.-H.; Ryu, S.-W. Controlled synthesis of GaN-based nanowires for photoelectrochemical water splitting applications. *Semicond. Sci. Technol.* **2016**, *32*, 013001. [CrossRef]
83. Li, Z.; Feng, S.; Liu, S.; Li, X.; Wang, L.; Lu, W. A three-dimensional interconnected hierarchical FeOOH/TiO_2/ZnO nanostructural photoanode for enhancing the performance of photoelectrochemical water oxidation. *Nanoscale* **2015**, *7*, 19178–19183. [CrossRef] [PubMed]
84. Sherman, B.D.; Ashford, D.L.; Lapides, A.M.; Sheridan, M.V.; Wee, K.-R.; Meyer, T.J. Light-Driven water splitting with a molecular electroassembly-based core/shell photoanode. *J. Phys. Chem. Lett.* **2015**, *6*, 3213–3217. [CrossRef]
85. Shaban, M.; Rabia, M.; El-Sayed, A.M.A.; Ahmed, A.; Sayed, S. Photocatalytic properties of PbS/graphene oxide/polyaniline electrode for hydrogen generation. *Sci. Rep.* **2017**, *7*, 1–13. [CrossRef]
86. Naldoni, A.; Guler, U.; Wang, Z.; Marelli, M.; Malara, F.; Meng, X.; Besteiro, L.V.; Govorov, A.O.; Kildishev, A.V.; Boltasseva, A.; et al. Broadband hot-electron collection for solar water splitting with plasmonic titanium nitride. *Adv. Opt. Mater.* **2017**, *5*, 1601031. [CrossRef]